Refractive Index of Liquid Water in Different Solvent Models

Kristian O. Sylvester-Hvid* and Kurt V. Mikkelsen

Department of Chemistry, H. C. Ørsted Institute, University of Copenhagen,
DK-2100 Copenhagen Ø, Denmark

Thomas M. Nymand

Hørretløkken 235, DK-8320 Mårslet, Denmark

Per-Olof Åstrand

Department of Chemistry, Norwegian University of Science and Technology, 7491 Trondheim, Norway

We present a combined molecular dynamics/quantum chemical perturbation method for calculating the refractive index of liquid water at different temperatures. We compare results of this method with the refractive index obtained from other solvent models. The best agreement with the experimental refractive index of liquid water and its temperature dependence is obtained using correlated gas-phase polarizabilities in the classical Lorentz−Lorenz expression. Also, the iterative self-consistent reaction field approach in the semicontinuum implementation matches the experimental refractive index reasonably well.

I. Introduction

The frequency-dependent refractive index, $n(\omega)$, of a material governs its potential applicability for various optical switching techniques.[1−6] From both a fundamental and an applied point of view, it is therefore crucially important to understand the refractive index and its microscopic, molecular origin. In this study, we attempt to model $n(\omega)$ for liquid water in the temperature range of 0−100 °C using various combinations of classical and quantum chemical solvent models. The optical properties of liquid water are of particular interest due to the strongly associated and hydrogen-bonded nature of the liquid. Water therefore poses a challenging benchmark system in the development of solvent models.

Understanding how molecular properties and chemical rates are affected by the surrounding medium has been the focus of many publications.[7−21] In particular, interpretation of measured macroscopic optical properties of liquids and solutions requires models for making a connection between the molecular property and the measured signal. Traditionally, this has been achieved using phenomenological models for the solute−solvent interactions.[22,23] In particular, the local field factors which assess the effective electromagnetic (EM) field experienced by the solute molecule have found widespread use. These classical approaches do not, however, include thermal fluctuations of the EM fields arising from the induced polarization in the solvent,[24−30] and temperature dependence enters only implicitly through the dielectric constant. Moreover, the use of local field factors implicitly assumes that the electro-optic properties of the solute are those of the gas-phase molecule. Clearly, it is necessary to describe how the electronic states of the solute are influenced by the surrounding solvent.[31−39] Attempts to do so include *ab initio* methods characterized as either continuum, supermolecu-

lar, or semicontinuum approaches.[31−39] In continuum models, the molecular monomer is enclosed in a cavity (usually spherical) of a linear, homogeneous, and isotropic dielectric and solvation is modeled by the polarization of this medium. In the supermolecular approach, solvation is modeled by the explicit inclusion of the first (and possibly second, third, ...) solvation shell in the *ab initio* calculation. The semicontinuum approach is the combination of the latter two and, thus, models solvation by including solvent molecules explicitly, and subsequently immersing the supermolecule in a dielectric medium.

It has been established that the continuum model for water fails to give a satisfying description of solvent effects since local, short-range interactions are not properly accounted for.[40−46] Hence, in this study, we use the supermolecular and the semicontinuum approaches to model the solvated water molecule. Note that the supermolecular model does not account for long-range interactions unless a large number of solvent molecules are included. Only the semicontinuum model includes both types of interactions but on the downside then involves a spherical cavity, the particular radius of which is not well defined.[47] With the nonequilibrium implementation of the iterative self-consistent reaction field (ISCRF) model,[48] this arbitrariness is eliminated such that semicontinuum computations may be performed with a unique cavity radius.

The models described above all consider solvation from a static point of view except for the use of temperature-dependent dielectric constants, and consequently fail to account for the temperature dependence at the molecular level. Attempts have been made to combine molecular dynamics (MD) (or statistical mechanical simulations in general) with supermolecular methods. This is done by extracting representative subsystems from MD simulations[49] performed at a given temperature and subsequently undertaking supermolecular (or semicontinuum) computations for individual subsystems. Approaching temper-

---

* To whom correspondence should be addressed. E-mail: ksh@theory.ki.ku.dk.

ature effects at the molecular level by this method is computationally demanding.

An alternative is to combine statistical mechanical simulations with *ab initio* quantum chemical calculations through perturbation theory. The merits of using intermolecular force fields constructed by intermolecular perturbation theory (IPT)[50−52] in molecular simulations[53,54] suggest that solvation for some properties can be treated as a perturbation of the gas-phase solute molecule. The gas-to-liquid shift of a molecular property can be expanded as a perturbation series, which contains products of property derivatives with respect to the perturbation and the magnitude of the perturbation.[55−59] The property derivatives can be determined from quantum chemical calculations (preferably by response theory) for the monomer, and statistical mechanical ensemble averages of the magnitude of the perturbation. Accordingly, concentration effects, which are very difficult (if not impossible) to handle in semicontinuum and supermolecular models, can also be determined, simply by performing the simulations at the concentration of interest. On the basis of MD simulations for pure bulk water, in this work we explore the IPT approach as an alternative route to studying the solvation of the water molecule.

This work is organized as follows. In section II, we present the theoretical background of the various methods applied in the calculation of the refractive index. In section III, we describe the details of the performed computations, and we present our results in section IV. We will discuss the results in section V.

Throughout, we conform to the CGS system of units.

II. Theoretical Background

A phenomenological approach to electric and magnetic effects in optically transparent materials is offered by analyzing the refractive index. The approach adopted here is based on classical electrodynamics, and treats the propagation of an EM field in a continuous medium. Solving the wave equation for a linear, homogeneous, and isotropic medium without any free charges gives for the frequency-dependent refractive index[60]

$$n(\omega) = \sqrt{[1 + 4\pi\chi_e(\omega)][1 + 4\pi\chi_m(\omega)]} \quad (1)$$

where χ_e and χ_m designate macroscopic linear electric and magnetic susceptibilities, respectively. Assuming additivity in terms of *effective*, average polarizabilities and magnetizabilities we have

$$n(\omega) = \sqrt{[1 + 4\pi N\alpha^{\text{eff}}(\omega)][1 + 4\pi N\xi^{\text{eff}}(\omega)]} \quad (2)$$

where $\alpha^{\text{eff}} = {}^1\!/_3(\alpha_{xx}^{\text{eff}} + \alpha_{yy}^{\text{eff}} + \alpha_{zz}^{\text{eff}})$ is the isotropic part of the molecular polarizability, ξ^{eff} the analogous magnetizability, and N the number density of the constituent molecules. On the microscopic level, these molecular properties can be derived by a variety of quantum mechanical methods.

However, from a phenomenological point of view, it is not entirely obvious how to establish a consistent link between eq 2 and quantum theory. One approximation is to adopt the framework of semiclassical radiation theory, where a spin-free molecular quantum system interacts with a prescribed EM field. The Hamiltonian for a molecule then is[61]

$$\mathscr{H} = \mathscr{H}_0 - \hat{\boldsymbol{\mu}}\cdot\mathbf{E}(t) - \hat{\mathbf{m}}\cdot\mathbf{B}(t) +$$
$$\frac{e^2}{8mc^2}\sum_i(\mathbf{r}_i\mathbf{r}_i - \mathbf{r}_i\cdot\mathbf{r}_i):\mathbf{B}(t)\mathbf{B}(t) - \frac{1}{2}\hat{\mathbf{Q}}:\nabla[\mathbf{E}(t)]_0 \quad (3)$$

where $\mathscr{H}_0$ is the nonrelativistic N-electron Hamiltonian and the summation is over electrons and where $\mathbf{E}$ and $\mathbf{B}$ designate electric and magnetic fields. The Hamiltonian in eq 3 is based on truncating the expansion of the vector potential after the linear term. Interactions linear in the EM field are due to the electric dipole operator ($\hat{\boldsymbol{\mu}} = e\sum_i\mathbf{r}_i$), the magnetic dipole operator ($\hat{\mathbf{m}} = {}^1\!/_2mc\sum_i\mathbf{l}_i$), and the second moment operator ($\hat{\mathbf{Q}} = e\sum_i\mathbf{r}_i\cdot\mathbf{r}_i$), the latter interacting with the gradient of the electric field. Quadratic interaction terms arise from the magnetic field only, and are due to the dynamic, diamagnetic term. Accordingly, time-dependent perturbation theory through second order in the fields, using eq 3, is the appropriate level of theory, consistent with a model for $n(\omega)$ in terms of α and ξ.

A collective analysis of electric and magnetic effects in terms of the refractive index is complex, however, due to the coupled nature of $\mathbf{E}$ and $\mathbf{B}$ in the EM field. The effects on $n(\omega)$ due to the magnetic interactions are generally small (especially for dielectric materials) but nonetheless require full account of eq 3, and hence also the quadrupole interactions.

Here we focus on the predominant electric interactions, neglecting magnetic effects altogether. A consistent level of theory thus is the *dipole approximation*, which corresponds to truncation of the vector potential before the linear term, leading to the interaction Hamiltonian[61]

$$\mathscr{H} = \mathscr{H}_0 - \boldsymbol{\mu}\cdot\mathbf{E}(t) \quad (4)$$

Apart from interaction with the radiation field as described by eq 4, in this study we are particularly concerned with the perturbation of the solute molecule due to its molecular surroundings. The approximation throughout this work is that these interactions are electrical in origin (except in the supermolecular model), and are either of an optical (electronic origin) or a static (all but electronic) nature. Therefore, the refractive index will be described in terms of electric perturbations of the water molecule, and analyzed correspondingly.

A. The Refractive Index. For materials subject to electrical polarization only, eq 2 is reduced to

$$n(\omega) = \sqrt{1 + 4\pi N\alpha^{\text{eff}}(\omega)} = \sqrt{1 + 4\pi Nf^C(\omega)\alpha^{\text{sol}}(\omega)} \quad (5)$$

where $\alpha^{\text{sol}}(\omega)$ is the average polarizability of the solvated molecule defined with respect to the cavity field given as $\mathbf{E}^C = f^C\mathbf{E}$ and

$$f^C = \frac{3\epsilon}{2\epsilon + 1} \quad (6)$$

where f^C is the cavity field factor. Here and throughout the text, ϵ is taken to be the optical dielectric constant ϵ_{op} related to the refractive index by the relation $n^2 = \epsilon_{\text{op}}$.

From a methodological point of view, the solvent effects contributing to α^{eff} may be accounted for either using classical models (as discussed, for example, in the monographs by Böttcher[22,23]) or by incorporating solvent effects directly in the quantum mechanical derivation of α^{sol}.

In classical continuum models, the molecular environment is introduced through the reaction field due to the polarization of the surrounding dielectric as induced by the permanent and induced electric moments of the solute molecule. In the simplest case of a nonpolar solute, the reaction field $\mathbf{E}^R = f^R\alpha(\mathbf{E}^C + \mathbf{E}^R)$ is due to the induced dipole moment where

$$f^R = \frac{1}{a^3}\frac{2(\epsilon - 1)}{2\epsilon + 1} \quad (7)$$

Refractive Index of Liquid Water

J. Phys. Chem. A, Vol. 109, No. 5, 2005 **907**

is the reaction field factor, a the cavity radius, and α the gas-phase polarizability of the solute molecule. In this picture, the effective solute polarizability is

$$\boldsymbol{\alpha}^{\text{eff}} = f^C(\mathbf{1} - f^R\boldsymbol{\alpha})^{-1}\,\boldsymbol{\alpha} \qquad (8)$$

and involves a product of the cavity field factor and a factor pertaining to the reaction field. The refractive index becomes

$$n(\omega) = \sqrt{1 + 4\pi N f^C(1 - f^R\alpha)^{-1}\,\alpha} \qquad (9)$$

which reduces to the familiar Lorentz−Lorenz expression[24]

$$n(\omega) = \sqrt{\frac{3 + 8\pi N\alpha(\omega)}{3 - 4\pi N\alpha(\omega)}} \qquad (10)$$

if a is eliminated using the Onsager approximation $4\pi Na^3 = 3$.[22] Equation 10 could also be the result of using $\alpha^{\text{eff}} = f^L\alpha$ directly in eq 5 where $f^L (=\epsilon + {}^2/_3)$ is the Lorentz field factor.[62] However, if this is done, the interpretation that eq 10 involves an optical reaction field contribution is not obvious, which may lead to inconsistent use. Within the classical framework, the average polarizability in eq 10 is the gas-phase polarizability. Hence, eq 10 does not account for the inertial (static) part of the solvent interactions to which the solute is subjected. The quantum mechanical derivation of α^{sol} must account for these interactions, and in this case, eq 5 should be employed to be consistent. However, for those quantum chemical solvation models in which the solvent interaction does not involve an optical reaction field, for example, the perturbation-based method presented below, eq 10 may still be used. In this case, the optical reaction field implied by eq 10 can be considered a supplementary and classical correction due to optical dielectric polarization of the solvent. For this same reason, α^{sol} derived using any of the SCRF-based quantum chemical methods should *not* be employed in eq 10 but rather in eq 5. In the latter case, the refractive index then becomes

$$n(\omega) = \frac{1}{16}\sqrt{\xi + (\xi + 8)^{1/2}} \qquad (11)$$

where $\xi = 1 + 12\pi N\alpha^{\text{sol}}$.

Considering the approximate nature of eq 10, it has been remarkably successful in the qualitative description of $n(\omega)$ for many nonpolar liquids based on gas-phase polarizabilities.[22,23] For such systems, the polarizability used in eq 10 is mainly due to electronic polarization, coupled to high-frequency vibrational modes of the molecular framework. For polar systems studied exclusively at optical frequencies, one may still use eq 10 using gas-phase polarizabilities with moderate success.[22,23] This is due to the inertial nature of the, otherwise quite substantial, contributions to the reorientational part of the polarization. Here we investigate eq 10 using both gas-phase α and α^{sol} based on static solvent perturbations, and eq 11 using α^{sol} including both static and optical perturbations.

B. Molecular Linear Response Properties. *Ab initio* computations of linear molecular response properties, within the solvent models of this study, can be realized using a Hamiltonian of the form[63]

$$\mathscr{H} = \mathscr{H}_0 + \bar{\mathscr{W}}_{\text{sol}} + \mathscr{V}(t) \qquad (12)$$

where $\bar{\mathscr{W}}_{\text{sol}}$ is the solvent interaction term particular to the model and $\mathscr{V}(t)$ describes the interaction between the solute system and the externally applied (but screened) EM field. The

latter is time-dependent and conveniently represented as the Fourier integral

$$\mathscr{V}(t) = \int_{-\infty}^{\infty}\mathrm{d}\omega\,\mathscr{V}^\omega\,\exp[(-i\omega + \eta)t] \qquad (13)$$

over Fourier components, $\mathscr{V}^\omega$, where η is a positive infinitesimal number which ensures that the perturbation is applied adiabatically; $\mathscr{V}(t \to -\infty) = 0$. In the absence of the perturbing field, the solute wave function is optimized according to the generalized Brillouin condition

$$\langle 0|[\lambda, \mathscr{H}_0 + \mathscr{W}_{\text{sol}}]|0\rangle = 0 \qquad (14)$$

to yield a reference state, $|0\rangle$, for the limit $t \to -\infty$. In eq 14, λ represents either orbital or configurational variation parameters. Subject to the field, that is for $t \geq 0$, the wave function of the solute molecule, $|\tilde{0}\rangle$, is propagated according to the Ehrenfest equations of motion. As described elsewhere,[64] the linear response equations are obtained and solved by considering the Ehrenfest equation to first order in the perturbing field. The perturbation expansion of the time dependence of the expectation value of a time-independent operator, A, is then

$$\langle A\rangle(t) = \langle 0|A|0\rangle + \int_{-\infty}^{\infty}\mathrm{d}\omega\,\exp[(-i\omega + \eta)t]\langle\langle A; \mathscr{V}^\omega\rangle\rangle_\omega \quad (15)$$

where $\langle\langle A; \mathscr{V}^\omega\rangle\rangle_\omega$ designates the linear response function given as[64]

$$\langle\langle A; \mathscr{V}^\omega\rangle\rangle_\omega = \sum_{n\neq 0}\frac{\langle 0|A|n\rangle\langle n|\mathscr{V}^\omega|0\rangle}{\omega - (\mathscr{E}_n - \mathscr{E}_0)} - \frac{\langle 0|\mathscr{V}^\omega|n\rangle\langle n|A|0\rangle}{\omega + (\mathscr{E}_n - \mathscr{E}_0)} \quad (16)$$

For an electric field, $\mathbf{E}_0\cos(\omega t)$, from eq 4 the corresponding Fourier components are

$$\mathscr{V}^\omega = -\frac{1}{2}\mathbf{E}_0\cdot\mathbf{r}[\delta(\omega - \omega_0) + \delta(\omega + \omega_0)] \qquad (17)$$

such that perturbation expansion of $\langle\boldsymbol{\mu}\rangle$ yields

$$\langle\boldsymbol{\mu}\rangle(t) = \boldsymbol{\mu}_0 + \boldsymbol{\alpha}(-\omega;\omega)\mathbf{E}_0\cos(\omega t) \qquad (18)$$

Therefore, we extract the solute polarizability tensor from the linear response function as $\boldsymbol{\alpha}(-\omega;\omega) = -\langle\langle\mathbf{r};\mathbf{r}^\omega\rangle\rangle$.

C. A Force Field Approach to Solvation. The fundamental assumption of the IPT approach is that the effect of the solvent for a molecular property, X, may be expressed as simply as

$$X^{\text{sol}} = X^{\text{vac}} + X^{\Delta\text{sol}} \qquad (19)$$

for example, as a perturbation of the gas-phase molecule. For calculations of the refractive index, the interesting property is $\alpha^{\text{sol}}(\omega)$, but to keep the notation simple, we will maintain the general formulation.

The solvent effect may be partitioned into various terms depending on the property under consideration. For polar liquids, electrostatic and dispersion interactions give the most important contributions to the solvation contribution of the linear molecular response properties. Thus, within the framework of IPT, we seek to compute components of the ensemble average of $\mathbf{X}^{\Delta\text{sol}}$ as[57−59]

$$\langle X_{\alpha\beta}^{\Delta\text{sol}}\rangle = \langle X_{E,\alpha\beta}\rangle + \langle X_{\omega,\alpha\beta}\rangle \qquad (20)$$

where the terms in the brackets denote an ensemble average. The electrostatic term, which is the most important term for polar liquids such as water, is expanded adopting a perturbative

approach (as, for example, has been done for nuclear shieldings[55,56])

$$\mathbf{X}_E = \mathbf{X}'_\gamma E_\gamma + \frac{1}{2}\mathbf{X}''_{\gamma,\delta} E_\delta E_\gamma + \dots + \mathbf{X}'_{\gamma\delta} E_{\gamma\delta} + \dots \quad (21)$$

where E_γ and $E_{\gamma\delta}$ are components of the electric field and the electric field gradient, respectively, due to the solvent. In eq 21, $\mathbf{X}'_\gamma$ and $\mathbf{X}''_{\gamma,\delta}$ are first and second derivatives of $\mathbf{X}$, respectively, with respect to the electric field, whereas $\mathbf{X}'_{\gamma\delta}$ is the first derivative with respect to the field gradient. Here and throughout this section, the Einstein summation notation is used. Previous investigations have shown that it is sufficient to include the contributions related to the linear and quadratic electric fields and the linear electric field gradient.[65-67]

To proceed, we impose the assumption of additivity for $\mathbf{X}$ in terms of atomic contributions $\mathbf{X} = \sum_k \mathbf{X}^k$, which is an old concept for polarizabilities.[68] Thus, in this distributed model, eq 21 may be applied to each component of the molecular property tensor, concerted with the statistical mechanical ensemble averages of the electric fields and field gradients. If the equation is truncated after the three most important terms, eq 21 becomes

$$\langle X_{E,\alpha\beta} \rangle = \sum_k \left(X'^k_{\alpha\beta,\gamma} \langle E^k_\gamma \rangle + \frac{1}{2} X''^k_{\alpha\beta,\gamma,\delta} \langle E^k_\delta E^k_\gamma \rangle + X'^k_{\alpha\beta,\gamma\delta} \langle E^k_{\gamma\delta} \rangle \right) \quad (22)$$

where k is the atom label. This approach is equivalent to our work presented in refs 69-71, where we have shown that using these parameter sets enables us to determine linear and nonlinear molecular optical properties.

The second contribution in eq 20 is the term originating from the dispersion interactions

$$\langle X_{D,\alpha\beta} \rangle = \frac{1}{2} X''^k_{\alpha\beta,\gamma,\delta} \langle E_0^2 \rangle^k_{\gamma\delta} \quad (23)$$

and is analogous to the terms used previously in the study of the chemical shift of water.[57] Here, the fluctuation potential acting on atom k is taken from the NEMO potential[51,57]

$$\langle E_0^2 \rangle^k_{\alpha\beta} = \sqrt{C} \frac{\bar{\omega}^A \bar{\omega}^B}{\omega^A + \bar{\omega}^B} \sum_j \alpha^j_{\gamma\delta} T^{kj}_{\alpha\gamma} T^{kj}_{\beta\delta} \quad (24)$$

where $\alpha^j_{\alpha\beta}$ is a component of the static polarizability tensor on atom j, $T^{kj}_{\alpha\beta}$ a component of the dipole-dipole interaction tensor $[\nabla_\alpha \nabla_\beta (1/R_{ij})]$, $\bar{\omega}^A$ an averaged ionization potential of molecule A, and C a factor of 1.89.

From eqs 22 and 23, we see that to arrive at the solvent shift for $\mathbf{X}$ the following is needed: (i) statistical mechanical ensemble averages of linear and quadratic electric fields, field gradients, and fluctuation potentials at all nuclei and (ii) derivatives of $\mathbf{X}$ with respect to the linear and quadratic electric field and its gradient, at all nuclei.

The ensemble averages of the field and field gradients, which perturb the solute molecule, are calculated from MD simulations of the liquid. These fields are static properties and are averaged over all molecules in the simulation volume. The required derivatives are obtained from quantum chemical calculations on the water monomer. However, the derivatives in eq 22 are not (to our knowledge) available in current electronic structure programs, and we turn to calculating these derivatives using the *point charge method*. Previously, this method has been used to calculate the corresponding atom-distributed derivatives of the molecular gradient and Hessian of water,[59] and the quad-

rupole shielding polarizabilities.[58] In the point charge method, we seek to represent the entire electrostatic solute−solvent interaction, in terms of configurations consisting of a solute molecule perturbed by sets of point charges. Here, we specifically employ mono- and dipole-perturbed solute configurations. For each such configuration (labeled i), we undertake an *ab initio* computation to obtain $^i\mathbf{X}$. Hence, $\bar{\mathscr{W}}'_{\text{sol}}$ in eq 12 simply accounts for the added charges.

A component of the property tensor for configuration i, according to eq 19, is the sum of the components of the vacuum tensor, $X^{\text{vac}}_{\alpha\beta}$, and a difference tensor, $^iX^{\Delta\text{sol}}_{\alpha\beta}$, representing the solvent shift in this equation, that is

$$^iX_{\alpha\beta} = X^{\text{vac}}_{\alpha\beta} + {}^iX^{\Delta\text{sol}}_{\alpha\beta} \quad (25)$$

Subsequently, the solvent shift tensor is expanded according to eq 21

$$^iX^{\Delta\text{sol}}_{\alpha\beta} = X'_{\alpha\beta,\gamma}{}^iE_\gamma + \frac{1}{2}X''_{\alpha\beta,\gamma,\delta}{}^iE_\delta{}^iE_\gamma + X'_{\alpha\beta,\gamma\delta}{}^iE_{\gamma\delta} \quad (26)$$

where the atom index has been omitted for clarity. In eq 26 lies the assumption that the Coulombic interactions alone are responsible for the change in the polarizability, and possible penetration effects are not considered. Such effects are rarely found for the point charge molecule distances adopted here, however. Finally, the parameters $X'_{\alpha\beta,\gamma}$, $X''_{\alpha\beta,\gamma,\delta}$, and $X'_{\alpha\beta,\gamma\delta}$ must be fitted to the set $\{^iX^{\Delta\text{sol}}_{\alpha\beta}, {}^iE_\gamma, {}^iE_{\gamma\delta}\}$ using a least-squares method. These fits are performed with a singular-value decomposition (SVD) method,[72] since the parameters are not independent. This concerns a small percentage only of the total number of parameters, and the dependence is rather small.

From eqs 22 and 23, it is clear that we have partitioned the problem of calculating $\mathbf{X}$ for the solute into two parts. One deals with the determination of the required ensemble averages. Note that the accounting of the many-body nature of the solvent is restricted to the evaluation of these averages. The other part deals with the calculation of the relevant derivatives. This latter part concerns the solute molecule only.

D. Nonequilibrium ISCRF Method. The nonequilibrium implementation of the ISCRF procedure[48] enables a consistent use of the self-consistent reaction Field (SCRF) solvation model[73] for pure liquids. By nature, the SCRF model relies on the assumption of infinite dilution. Modeling a pure liquid as a solute, solvated by identical molecules, this assumption naturally breaks down. The remedy is to impose a self-consistent procedure, coupling the *microscopic* and quantum-based SCRF model to a *macroscopic* and classical model for the optical dielectric function, the latter taking molecular optical properties as input. We investigate two macroscopic models for the optical dielectric constant $\epsilon_{\text{op}}(\omega) = n^2(\omega)$, namely, the Lorentz−Lorenz expression in eq 10 and the expression in eq 11 based solely on the cavity field.

In the SCRF model, the solute, as represented by its wave function and corresponding charge distribution, is situated inside a spherical cavity of a homogeneous, isotropic, and linear dielectric medium. The radius of this cavity is R_{cav}, and the dielectric extends to infinity and solely is characterized by its optical, $\epsilon_{\text{op}}(\omega,T)$, and static dielectric constant, $\epsilon_{\text{st}}(T)$. The solute charge distribution, formally multipole-expanded to order l, induces a polarization state in the dielectric represented by the polarization vector

$$\mathbf{P} = \mathbf{P}_{\text{op}} + \mathbf{P}_{\text{in}} \quad (27)$$

Refractive Index of Liquid Water

J. Phys. Chem. A, Vol. 109, No. 5, 2005 **909**

The decomposition into an optical and an inertial component reflects the two extreme time scales approximating the non-equilibrium solvent dynamics, namely, infinitely fast and infinitely slow processes. The electronic solvent degrees of freedom, represented by $\mathbf{P}_{op}$, may respond instantaneously to changes in the solute molecular charge distribution. Therefore, the electronic solvent modes are always in equilibrium with the solute electronic subsystem. $\mathbf{P}_{in}$, which responds infinitely slowly to changes in the molecular charge distribution, accounts for all other solvent degrees of freedom but the electronic. Prior to the EM perturbation, the solute−solvent system is equilibrated by demanding eq 14 be fulfilled for[63]

$$\mathcal{W}_{sol} = \sum_{lm} g_l(\epsilon_{st})(T^n_{lm})^2 - 2\sum_{lm} g_l(\epsilon_{st})\langle 0|T_{lm}|0\rangle T_{lm} \quad (28)$$

which in turn defines the reference state, $|0\rangle$, and the inertial polarization state of the solvent. In eq 28, $T_{lm} = T^n_{lm} - T^e_{lm}$ and T^n_{lm} and T^e_{lm} designate the nuclear and electronic contributions to the multipole charge moments, respectively. For a spherical cavity, the polarization fields due to the induced polarization charges in the dielectric medium are

$$R_{lm}(\epsilon_{op}) = g_l(\epsilon_{op})\langle \tilde{0}|T_{lm}|\tilde{0}\rangle \quad (29)$$

and

$$R_{lm}(\epsilon_{st},\epsilon_{op}) = g_l(\epsilon_{st},\epsilon_{op})\langle 0|T_{lm}|0\rangle \quad (30)$$

The reaction field factors, $g_l(\epsilon)$, are given as

$$g_l(\epsilon) = -\frac{1}{2}R_{cav}^{-(2l+1)}\frac{(l+1)(\epsilon-1)}{l+\epsilon(l+1)} \quad (31)$$

with

$$g_l(\epsilon_{st},\epsilon_{op}) = g_l(\epsilon_{st}) - g_l(\epsilon_{op}) \quad (32)$$

If the EM perturbation is applied, the solute state is propagated subject to the reaction field, as characterized by the constant inertial polarization, $\mathbf{P}_{in}$, the equilibrated optical polarization, $\mathbf{P}_{op}$, and the state-dependent solvent interaction operator[63,73−75]

$$\tilde{\mathcal{W}}_{sol} = \sum_{lm} g_l(\epsilon_{op})(T^n_{lm})^2 + \sum_{lm} g_l(\epsilon_{op},\epsilon_{st})(T^n_{lm})^2 - \\ 2\sum_{lm} g_l(\epsilon_{op})\langle \tilde{0}|T_{lm}|\tilde{0}\rangle T^e_{lm} - 2\sum_{lm} g_l(\epsilon_{op},\epsilon_{st})\langle 0|T_{lm}|0\rangle T^e_{lm} \quad (33)$$

The resulting nonequilibrum SCRF linear response properties are parametrized with respect to ϵ_{op}, ϵ_{st}, and R_{cav}.

The ISCRF procedure is initiated by computing $\alpha^{sol}(\omega)[\epsilon_{op},\epsilon_{st},R_{cav}]$ based on ϵ_{op} derived using either eq 10 or 11 and gas-phase polarizabilities. ϵ_{st} is taken to be the experimental values and R_{cav} chosen as in normal SCRF computations. The resulting α^{sol} is then used to update ϵ_{op} according to eq 10 or 11, which then serves as input to the next SCRF step. Continuing this iterative scheme until convergence yields a self-consistent determination of corresponding microscopic (α^{sol}) and macroscopic (ϵ_{op}) optical properties for the solute−solvent system, parametrized now only with respect to $\epsilon_{st}(T)$ and R_{cav}. However, R_{cav} is quite arbitrary in the SCRF model. In the ISCRF scheme, this arbitrariness is eliminated considering R_{cav} as a free parameter, characteristic of the solute−solvent system, the solvent model, and the level of theory. Elimination is done by finding the particular value of R_{cav} which makes the ISCRF-determined α^{sol} reproduce the experimental refractive index,

$^{ex}n(\omega)$, at a particular frequency. We refer to this as calibration of the ISCRF procedure, performed at the particular calibration frequency, yielding the calibration value of R_{cav}.[48]

III. Computational

A. Molecular Dynamics Simulations. When ensemble averages of electric fields and field gradients are calculated as required in eqs 22 and 23, it is crucial that the electrostatics of the liquid are accurately modeled. This can be achieved conveniently by constructing the force fields using perturbation theory.[50] The NEMO potential with its atomic dipole moments and atomic anisotropic polarizability tensors[76] is a force field based on this idea. We used MOLSIM[77] with this potential to perform MD simulations to obtain the required ensemble averages. The simulated system consists of 216 water molecules enclosed in a cubic box. The forces were calculated using a spherical cutoff of 9.3 Å, and the induced dipole moments were calculated using a combined first-order predictor with a full self-consistent solution.[78] The NVT ensemble was achieved by scaling the velocities,[79] and the equations of motion of the rigid molecules were integrated using quaternions[80] and the velocity version of the Verlet algorithm,[81] with a time step of 2 fs. The system was equilibrated for 10 ps at each temperature before data was collected for 150 ps. Simulations were performed between 0 and 100 °C with 10 °C intervals employing experimental densities.

B. *Ab Initio* Polarizabilities. All *ab initio* electronic structure computations were undertaken with the DALTON program package.[82] Linear response computations of dynamic polarizabilities at the common laser frequencies of 1064, 800, 632.8, 589, 337, and 193 nm were performed for the following three solvent models.

(i) Point Charge Method. SCF and MCSCF computations for the water monomer surrounded by various configurations of point charges.

(ii) Supermolecular Method. SCF computations for the water monomer surrounded by its first solvation shell.

(iii) Semicontinuum Method. ISCRF computations for the water monomer surrounded by its first solvation shell.

In the point charge method, the water monomer at the experimental C_{2v} geometry ($r_{OH} = 0.957541$ Å, $\theta_{HOH} = 104.516°$) was placed in the $x-z$ plane with the z-axis as the C_2 axis and the hydrogen atoms at $\{\pm x,0,+z\}$. Point charge configurations consisted of either a single negative point charge or a negative and a positive charge, arranged to form a dipole with direction toward the oxygen atom. To avoid charge transfer effects, the negative point charges were placed closest to the water molecule. All charges were given a magnitude of 1 au. Monopole configurations with r_{OQ} equal to 4.5, 5.0, and 5.5 au and dipole configurations with r_{OQ_-} equal to 4.0 au and r_{OQ_+} equal to 4.5 and 5.0 au were used. For each of these five possibilities, a number of configurations were generated for which the angle, ϕ, between $\mathbf{r}_{OQ}$ and $\mathbf{r}_{HH}$ was either 0°, 45°, or 90°. For each choice of ϕ, the angle between $\mathbf{r}_{OQ}$ and the molecular dipole axis was allowed to vary between 0° and 180°. This procedure generated configurations with either C_{2v}, C_s, or no symmetry. For each non-C_{2v} configuration, the configurations also generated by applying the C_{2v} reflection symmetry operations on the charge position vectors were included. Hartree−Fock (HF) computations for every configuration generated in this way were performed with a modest and a large size ANO basis set, as given by Widmark et al.[83,84] The smaller basis set (ANO-S) consists of a [10s6p3d/4s3p1d] contraction on O and [6s4p/3s2p] on H, and gives an E^{vac}_{HF} of -76.056110 au. The

TABLE 1: The ISCRF Procedure Requires Only the Density and Static Dielectric Constant ϵ_{st} as Input at a Given Temperature T^a

	$T = 20\ °C$	$T = 100\ °C$
n_D	1.33335	1.31819
density (g/cm^3)	0.99823	0.95840
ϵ_{st}	80.37	55.51
R_{cav}^L (au)	7.56242	7.5533
R_{cav}^C (au)	7.51150	7.50570

^{a} Also given are the cavity radii which reproduce ^{ex}n(589 nm) using the ISCRF(L) and ISCRF(C) models at 20 and 100 °C.

larger set (ANO-L) has contractions, [14s9p4d3f/5s4p3d2f] for O and [8s4p3d/4s3p2d] for H, for which $E_{HF}^{vac} = -76.066866$ au. The HF procedure was converged to 10^{-6} au and integrals evaluated in a spherical harmonic basis and with a threshold of 10^{-15} au.

Complete active space (CAS) computations were undertaken with the well-established $6a_1$, $3b_1$, $3b_2$, $1a_2$ active space with 1s on O held inactive, and initiated from MP2 natural occupation numbers. CAS computations were performed for the ANO-L basis set only, and the wave functions converged to 10^{-9} au, with respect to the energy gradient.

Computations involving point charges were more susceptible to convergence problems than the corresponding vacuum computations. Therefore, for representative configurations subject to large perturbations on the water molecule, convergence tests were carried out. For such configurations, finite field-derived static polarizabilities were compared with the corresponding polarizabilities obtained from linear response computations. The thresholds as given above were chosen according to these tests.

Supermolecular computations were performed for the water molecule surrounded by its first solvation shell (a water pentamer) and the empty solvation shell (a water tetramer).[40] The individual monomers have identical geometry ($r_{OH} = 0.958019$ Å, $\theta_{HOH} = 104.500°$), and the symmetry of both the pentamer and tetramer is C_{2v}, referring to the same frame that was used for the point charge method. Computations were undertaken only for the ANO-L set, which for the pentamer gave an E_{HF}^{vac} of -380.355238 au and an E_{HF}^{vac} of -304.268662 au for the tetramer. Linear response properties for the central (solvated) water molecule were obtained using the differential shell method; i.e., $\alpha^{sol} = \alpha_{pentamer} - \alpha_{tetramer}$.[40]

Semicontinuum computations were carried out within the ISCRF framework by undertaking nonequilibrium SCRF computations for the water penta- and tetramer using identical cavity radii. ISCRF procedures were established by computing polarizabilities at 589 nm (the Na D-line) using static dielectric constants for 293.15 and 373.15 K, and extracting α^{sol} by the differential shell approach.[40] The ISCRF procedure was considered to be converged when polarizabilities in consecutive SCRF steps differed by less than 0.001 au. Each SCRF computation employed a formal multipole expansion to order $l = 9$, and the linear response equations were solved to within a threshold of 10^{-5} au. At each temperature, two ISCRF procedures were adopted, the first based on eq 10, termed ISCRF(L), and the second based on eq 11, termed ISCRF(C). For each of the four cases, multiple ISCRF computations were conducted for a range of cavity radii to find R_{cav} which makes the particular ISCRF scheme reproduce the refractive index of water[85] at 589 nm, at the relevant temperature. The cavity radii thus found, and which calibrate each of the ISCRF procedures, are listed in Table 1 along with the input used for these

TABLE 2: Polarizability in Atomic Units at 589 nm Calculated Using the IPT Model

$T\ (°C)$	$\langle\alpha^{\Delta sol}\rangle^a$				$\langle\alpha^{sol}\rangle^b$	α^{vac}
	LF^c	QF^d	LFG^e	D^f		
	HF/ANO-S					7.654
20	−0.602	0.353	0.0512	0.880	8.336	
60	−0.541	0.298	0.0427	0.804	8.258	
100	−0.486	0.253	0.0358	0.736	8.191	
	HF/ANO-L					8.627
20	−0.509	0.580	0.0296	1.334	10.062	
60	−0.458	0.489	0.0250	1.226	9.910	
100	−0.412	0.414	0.0210	1.127	9.777	
	CAS/ANO-L					9.473
20	−0.659	0.825	0.0489	1.927	11.615	
60	−0.592	0.696	0.0414	1.772	11.389	
100	−0.533	0.590	0.0348	1.628	11.192	

^{a} Equal to $\frac{1}{3}(\langle\alpha_{xx}^{\Delta sol}\rangle + \langle\alpha_{yy}^{\Delta sol}\rangle + \langle\alpha_{zz}^{\Delta sol}\rangle)$. ^{b} $\alpha^{vac} + \frac{1}{3}(\langle\alpha_{xx}^{\Delta sol}\rangle + \langle\alpha_{yy}^{\Delta sol}\rangle + \langle\alpha_{zz}^{\Delta sol}\rangle)$. ^{c} The linear field contribution. ^{d} The quadratic field contribution. ^{e} The linear field gradient contribution. ^{f} The dispersion contribution.

computations. Using input from Table 1, subsequent nonequilibrium ISCRF computations of α^{sol} were carried out at the other frequencies. Clearly, the time-consuming step is the optimization of R_{cav} for each ISCRF scheme, and to limit computational costs, the SCRF computations were performed with the smaller ANO-[432/32] basis set. Problems concerning basis set superposition errors have been addressed previously[40] and were found not to pose a significant problem.

IV. Results

A. IPT Polarizabilities. In the IPT approach, the dynamic polarizability tensor is calculated from eqs 22 and 23. In Table 2, we present values for the various contributions to the isotropic part of the polarizability tensor at 589 nm, for the HF/ANO-S, HF/ANO-L, and CAS/ANO-L levels of theory. LF, QF, LFG, and D designate the linear field, quadratic field, linear field gradient, and dispersion contributions, respectively. These are presented at three representative temperatures. We note that all contributions (LF, QF, LFG, and D) decrease in magnitude with an increase in temperature. This is a consequence of the fact that the electric fields, field gradients, and the fluctuation potential all decrease with an increase in temperature. For both the HF and CAS calculations, we note that the LF and QF terms are of opposite sign and similar magnitude, and the CAS QF terms are larger than the HF QF terms. At all levels of theory, the LFG terms are an order of magnitude smaller than the LF and QF terms, with an altered sign relative to the LF terms. The importance of higher-order terms related to the electric field, going beyond the contributions to the quadratic electric field, has previously been determined to be insignificant.[65−67] The dispersion contributions have the same sign as the QF terms and are larger by a factor of 2, and thus dominate α^{sol} because of the opposite signs of the LF and QF terms. The D and QF terms increase by ∼50% as we move from the ANO-S to the ANO-L basis set, reflecting the increasing diffusiveness of the molecular electron distribution as the one-electron space is expanded. From Table 2, another ∼50% increase in the D and QF terms can be attributed to electron correlation. For reference, the corresponding gas-phase polarizabilities for 589 nm are 7.654, 8.627, and 9.473 au at the HF/ANO-S, HF/ANO-L, and CAS/ANO-L levels of theory, respectively. Hence, the IPT method leads to positive solvent shifts as such.
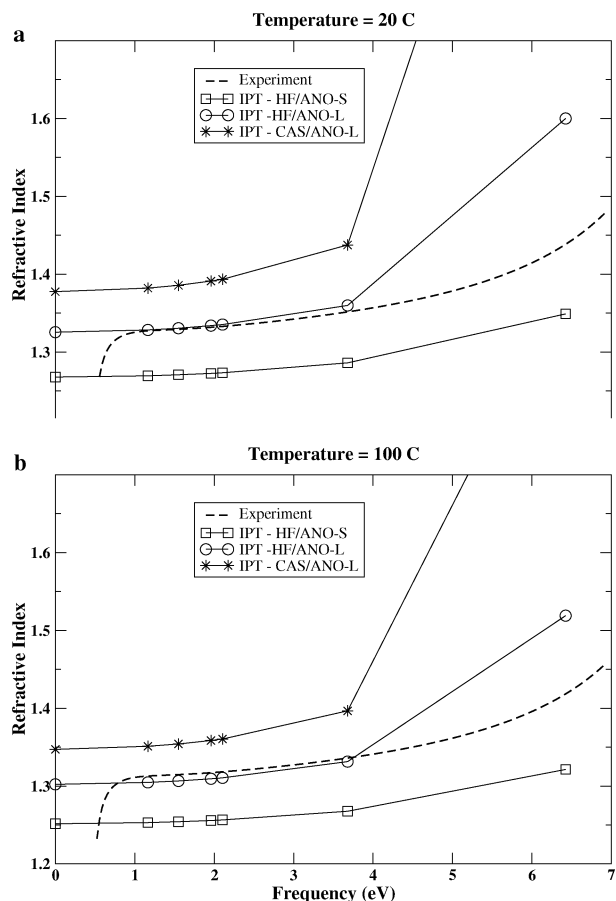
Refractive Index of Liquid Water

J. Phys. Chem. A, Vol. 109, No. 5, 2005 **911**

Figure 1. Dispersion of the refractive index, calculated from eq 10 with IPT polarizabilities, and compared with $^{ex}n(\omega)$.[85] (a) Dispersion at 20 °C and the missing data point at $n(6.42\ eV) = 2.28$. (b) Dispersion at 100 °C and the missing data point at $n(6.42\ eV) = 1.95$.

Figure 2. Dispersion of the refractive index calculated from eq 10 and the ($\diamond$) supermolecule in the differential shell approach at the HF/ANO-L level, ($+$) the gas-phase monomer at the CAS/ANO-L level, ($\times$) the ISCRF(L)/differential shell approach at the HF/ANO[432/32] level, and ($\odot$) the IPT method at the HF/ANO-L level. For the ISCRF(C)/differential shell approach at the HF/ANO[432/32] level ($\triangle$), the refractive index was obtained from eq 11. In panel a, the dispersion is displayed for 20 °C, and in panel b, it is displayed for 100 °C.

B. Refractive Index. We calculated the dispersion for $n(\omega)$ in the optical transparent region (from 1064 to 193 nm) employing polarizabilities from the different solvent models. In Figure 1, we display the performance of the IPT model at 20 (a) and 100 °C (b), based on eq 10 along with the experimental refractive index, $^{ex}n(\omega)$. At the HF level, using the ANO-S basis set, $^{ex}n(\omega)$ is underestimated, but the dispersion is reproduced reasonably well. With the larger ANO-L set, results for $n(\omega)$ are quite close to those from the experiment, in particular for 20 °C. However, the dispersion then is exaggerated at high frequencies. Using the CAS/ANO-L polarizabilities for calculating $n(\omega)$ overshoots $^{ex}n(\omega)$ and makes the dispersion description even worse as seen from Figure 1. Closer investigation of the CAS results revealed difficulties in converging the linear response equations for some water point charge configurations at the highest frequency. For these configurations, unphysically large polarizabilities were obtained, leading to the extreme dispersion seen in Figure 1. We refer to this problem as *absorption* and return to the issue below.

Comparing panels a and b of Figure 1, we see that the effect of an increased temperature is a downward shift in $n(\omega)$. Most affected are results based on CAS/ANO-L polarizabilities, and the least affected are those based on HF/ANO-S polarizabilities.

In Figure 2, we compare $n(\omega)$ at 20 (a) and 100 °C (b), derived using the different solvent models investigated in this study. In all but the ISCRF cases, $n(\omega)$ was obtained using eq 10, and for the IPT approach, only the HF/ANO-L results are displayed as these reproduced the values from experiment quite well.
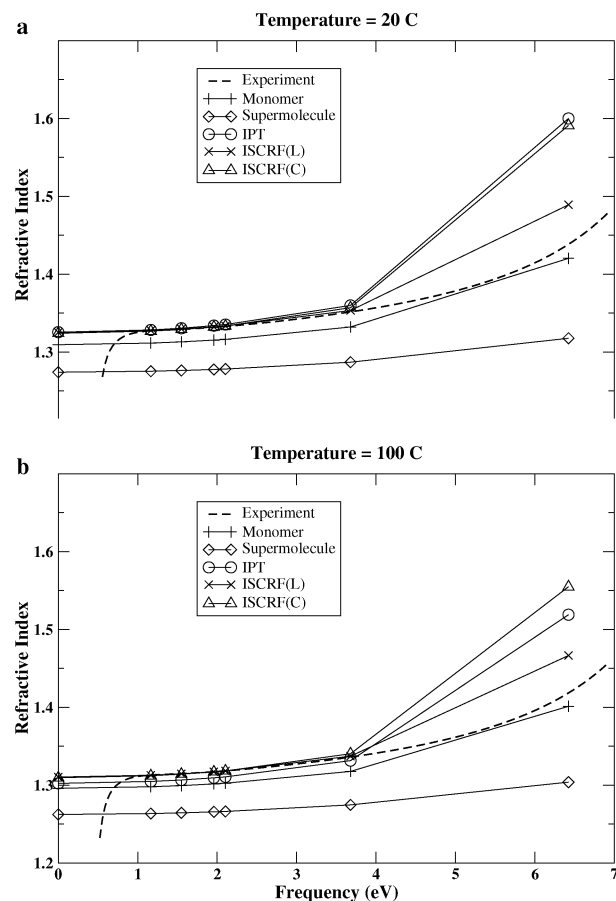
Using HF/ANO-L polarizabilities obtained with the supermolecular differential shell approach, the computed refractive index ($\diamond$) clearly underestimates the experimental data at both temperatures. Also, as seen from Figure 2, only in the supermolecular approach is the dispersion underestimated. In this approach, only the short-range solvent interactions (the first solvation shell) are included in the computations of α^{sol}. Long-range optical solvent interactions are included, but only in an implicit fashion by virtue of using eq 10 to derive $n(\omega)$. Without doubt, accounting for electron correlation (using, for example, coupled cluster methods) in the supermolecular approach would improve its performance.[86−88]

With the ISCRF(L) and ISCRF(C) procedures, the refractive index at 589 nm (n_D) is trivially reproduced as this was chosen as the calibration frequency. The performance of the ISCRF procedure, therefore, should be judged on its ability to give the correct dispersion. From Figure 2, we see that at low frequencies both the ISCRF(L) and ISCRF(C) procedures are quite satisfactory in this respect, whereas at the highest frequency, the dispersion is exaggerated to an extent similar to the IPT results. In fact, at 100 °C the ISCRF(C) procedure performs worse than the IPT model in terms of dispersion. We stress that only the ISCRF(C) procedure represents a consistent coupling of micro- and macroscopic solvent models. With the ISCRF(L) model, the reaction field is included both in the SCRF derivation of α^{sol} and in the reaction field factor leading to eq 10. This is
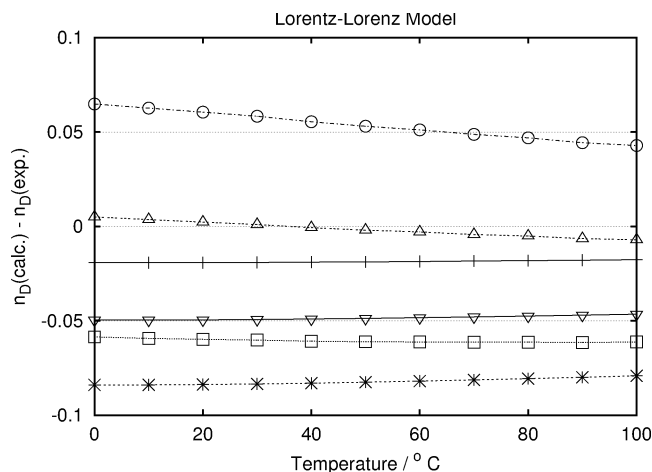
Figure 3. Shift in the refractive index relative to experiment at 589 nm vs temperature. Shifts have been obtained using IPT and gas-phase polarizabilities in eq 10: (⊙) IPT-CAS/ANO-L, (△) IPT–HF/ANO-L, (□) IPT-HF/ANO-S, and for the gas-phase numbers, (+) CAS/ANO-L, (▽) HF/ANO-L, and (∗) HF/ANO-S.

inconsistent. The double counting of the reaction field, and thus the exaggerated solvent polarization response for the ISCRF(L) model, leads to larger values of the cavity radii required to calibrate the ISCRF(L) procedure than in the ISCRF(C) procedure, as confirmed in Table 1. The smaller cavity radii implied by the ISCRF(C) model, however, make subsequent SCRF response computations of α^{sol} at the highest frequency more susceptible to the absorption problem, as clearly evidenced in Figure 2. Hence, although inconsistent, the ISCRF(L) model seems to give the better performance in terms of reproducing the value from experiment.

To inquire about the necessity of including the solvent interaction in the quantum chemical derivation of α^{sol}, in Figure 2 we display $n(\omega)$ derived from eq 10 and gas-phase CAS/ANO-L polarizabilities for the water monomer. Using the Lorentz internal field correction to entirely represent the solvent interactions works surprisingly well in terms of reproducing the values from experiment. At both temperatures, this method consistently underestimates the experimental data by ∼0.2, but of the models that have been investigated, it gives the best dispersion description.

Generally, the effect of increasing the temperature from 20 to 100 °C is a downward shift of $n(\omega)$, as seen in panels a and b of Figure 2.

In the IPT model for the solvent environment, the temperature dependence of $n(\omega)$ enters through both $N(T)$ and α^{sol}. In Figure 3, we display the temperature dependence of n_D, relative to the corresponding experimental value. We refer to this quantity as $\Delta n_D(T)$, and give results obtained using IPT and gas-phase polarizabilities in eq 10. The extent to which our results show the correct temperature dependence is thus a matter of the slope and displacement from zero of the $\Delta n_D(T)$ curves in Figure 3. The gas-phase results depend on temperature only through $N(T)$, which gives rise to a decreasing $\Delta n_D(T)$ with T in Figure 3. Among the gas-phase results, we obtain an almost perfect temperature description using CAS/ANO-L polarizabilities in eq 10 over the entire temperature interval. With temperature-dependent IPT polarizabilities in eq 10, from Figure 3 we observe decreasing slopes of $\Delta n_D(T)$ for the CAS/ANO-L and HF/ANO-L cases, whereas for the HF/ANO-S case, $\Delta n_D(T)$ is nearly independent of T. Judging from the vertical displacement of $\Delta n_D(T)$ in Figure 3, it is again clear how well the IPT–HF/ANO-L polarizabilities reproduce the experimental value for

n_D. The temperature dependence, however, is described better in the HF/ANO-S case. The general observation from Figure 3 is that introducing temperature effects into α^{sol} via the IPT approach leads to excessive temperature sensitivity of the computed refractive index, and that introducing temperature dependence only through $N(T)$ in eq 10 reproduces the experimental temperature dependence quite well.

V. Discussion

With the IPT approach, to a large extent we are able to reproduce $^{ex}n(\omega)$ up to ∼4 eV using HF/ANO-L polarizabilities. The fact that including electron correlation leads to a general overestimation of the experiment indicates, however, that IPT as used here exaggerates the solvent shift. Most likely, this is due to the dominating dispersion term in the expansion of the solvent shift, which should be balanced by a negative exchange repulsion term not included in the current approach. Despite that, higher-order terms are less significant,[65−67] the magnitude of the LF and QF terms still imply a slow convergence of the power series expansion of the solvent shift, and thus we are not accounting for the entire electrostatic interaction. Also, it should be pointed out that eq 24 is a rather crude approximation for the fluctuation potential, and eq 23 in fact should include an integration over the frequency space. Thus, we include a static solvation term that in principle is frequency-dependent.

Another reason for overestimating the refractive index could be the approximate nature of eq 10. Using eq 5 where $\alpha^{eff} = \alpha^{sol}$, on the other hand, leads to dispersion curves for the refractive index (not shown here) much below the $^{ex}n(\omega)$. Qualitatively, the difference between eqs 5 and 10 is that the Lorentz−Lorenz model includes the screening of the Maxwell field (i.e., the cavity field) and a dipolar optical reaction field. The first contribution must be included irrespective of the microscopic solvent model used. Including the second contribution is consistent only if α^{sol} includes entirely static solvent perturbations, as is the case for the IPT approach. However, the magnitude of the optical reaction field implied by eq 10 may well lead to an exaggerated polarization response and thus refractive index.

The temperature dependence of the refractive index calculated in the IPT model is reflected in the interplay of the temperature-dependent contributions in Table 2. Hence, the improved temperature description seen in Figure 3 moving from CAS/ANO-L to HF/ANO-L to HF/ANO-S is mainly attributed to a corresponding decrease in the temperature dependence of the dispersion terms in Table 2. However, comparing the temperature description resulting alone from eq 10, as used with temperature-independent α^{vac}, clearly illustrates the importance of balancing the expansion terms correctly. In this respect, the IPT approach adopted here calls for further improvements, but nonetheless illustrates its applicability in terms of deriving temperature-dependent solute polarizabilities. Access to analytic derivatives, as required by the perturbation expansion, would also strengthen the IPT method, as we would avoid the absorption problem seen at high frequencies, being mainly an artifact of the point charge method.

Computing the refractive index based on supermolecular polarizabilities, for which only interactions with the first solvation are accounted (apart from the optical reaction field due to eq 10), gives results that do not reproduce $^{ex}n(\omega)$. Considering that the corresponding monomer computations at the HF level (not shown here) perform even worse, together with the fact that the monomer CAS/ANO-L results are within 0.2 of $^{ex}n(\omega)$, points to electron correlation as the important

Refractive Index of Liquid Water

J. Phys. Chem. A, Vol. 109, No. 5, 2005 **913**

issue. Hence, the supermolecular approach would most likely describe the magnitude of the refractive index much better using a correlated method. Vibrational contributions are known to increase α.[89-91] Their contribution, however, can hardly justify an increase of 0.2 in the refractive index needed to bring the monomer CAS/ANO-L results up to $^{ex}n(\omega)$, and does by no means explain the poor result obtained with the supermolecular model. The CAS/ANO-L gas-phase polarizabilities are of such quality that the polarization contribution lacking to reproduce $^{ex}n(\omega)$ most likely is due to the absence of the solvent perturbation. This contribution is surprisingly small which again might indicate that the Lorentz−Lorenz model compensates for a lacking solvent perturbation at the microscopic level.

Within the ISCRF models, both optical and static solvent perturbations are identified by virtue of the nonequilibrium SCRF computations of α^{sol}. As the SCRF procedure includes an optical reaction field, we should use eq 11 to consistently establish the ISCRF procedure.[92] The dispersion description below ∼4 eV for the ISCRF(C) model is comparable to that of the IPT-HF/ANO-L model, at both temperatures that were investigated. At the highest frequency, the method is also subjected to the absorption problem, in this case, however, due to a small cavity radius as required by the calibration to n_D. Double counting of the optical reaction field and using eq 10 instead, although inconsistent, improves the dispersion description; i.e., the exaggerated optical polarization response allows for a larger cavity radius for the calibration of the ISCRF(L) procedure. Although not evident from the magnitude of the refractive index, the ISCRF procedure would also improve upon introduction of electron correlation. The reason is that if α^{sol} is increased at the calibration frequency due to correlation, then the calibration could be obtained for a larger cavity radius. Consequently, the perturbation stress on the solute system is reduced and the absorption problem less pronounced at high frequencies.

In summary, we have demonstrated that the solvent shift at different temperatures can be described using the IPT approach, but that caution should be exercised when truncating the perturbation expansion of the solvent shift of the polarizability. Using the supermolecular model at the HF level does not account for the refractive index in a satisfactory way. The ISCRF model in both a consistent and inconsistent implementation accounts well for the refractive index below ∼4 eV at the HF level. At higher frequencies, the ISCRF procedures exaggerate the dispersion probably due to a lack of electron correlation. Finally, using high-quality gas-phase polarizabilities computed for the water monomer reproduces the experimental refractive index and its temperature dependence surprisingly well when the Lorentz−Lorenz expression is employed.

References and Notes

(1) McAulay, A. D. *Optical Computer Architectures*; Wiley: New York, 1991.

(2) Miller, D. A. B. *Opt. Photonics News* **1990**, *1*, 7.

(3) Killer, H. B. *Fiber Optic Communications*; Prentice Hall: Englewood Cliffs, NJ, 1991.

(4) Senior, J. M. *Optical Fiber Communications*; Prentice Hall: Englewood Cliffs, NJ, 1983.

(5) Agrawal, G. P. *Nonlinear Fiber Optics*; Academic Press: New York, 1989.

(6) Solymar, L.; Webb, D. J.; Grunnet-Jepsen, A. *The Physics and Application of Photorefractive Materials*; Oxford University Press: Oxford, U.K., 1996.

(7) Lienau, C.; Zewail, A. H. *J. Phys. Chem.* **1996**, *100*, 18629.

(8) Wan, C.; Gupta, M.; Baskin, J. S.; Kim, Z. H.; Zewail, A. H. *J. Chem. Phys.* **1997**, *106*, 4353.

(9) Jimenez, R.; Fleming, P. V. K. G. R.; Maroncelli, M. *Nature* **1994**, *369*, 471.

(10) Horng, M. L.; Gardecki, J. A.; Papazan, A.; Maroncelli, M. *J. Phys. Chem.* **1995**, *99*, 17311.

(11) Chudoba, C.; Lutgen, S.; Jentsch, T.; Riedle, E.; Woerner, M.; Elsaesser, T. *J. Phys. Chem.* **1995**, *99*, 17311.

(12) Fonseca, T.; Kim, H. J.; Hynes, J. T. *J. Mol. Liq.* **1994**, *60*, 17311.

(13) Staib, A.; Borgis, D.; Hynes, J. T. *J. Chem. Phys.* **1995**, *102*, 2487.

(14) Eisenthal, K. B. *J. Phys. Chem.* **1996**, *100*, 12997.

(15) Hayashi, S.; Ando, K.; Kato, S. *J. Phys. Chem.* **1995**, *99*, 955.

(16) Kahlow, M. A.; Kang, T.; Barbara, P. F. *J. Chem. Phys.* **1988**, *88*, 2372.

(17) Kahlow, M. A.; Jarzeba, W.; Kang, T.; Barbara, P. F. *J. Chem. Phys.* **1989**, *90*, 151.

(18) Tomasi, J.; Persico, M. *Chem. Rev.* **1994**, *94*, 2027.

(19) Mikkelsen, K. V.; Kmit, M. *Theor. Chim. Acta* **1995**, *90*, 307.

(20) Reichardt, C. *Solvents and Solvent Effects in Organic Chemistry*; VCH: Weinheim, Germany, 1988.

(21) Newton, M. D.; Sutin, N. *Annu. Rev. Phys. Chem.* **1984**, *35*, 437.

(22) Böttcher, C. J. F. *The Theory of Electric Polarization*; Elsevier: Amsterdam, 1984; Vol. I.

(23) Böttcher, C. J. F.; Bordewijk, P. *The Theory of Electric Polarization*; Elsevier: Amsterdam, 1984; Vol. II.

(24) Lorentz, H. A. *The Theory of Electrons*, 2nd ed.; Dover: New York, 1952.

(25) Onsager, L. *J. Am. Chem. Soc.* **1936**, *58*, 1486.

(26) Wortman, R.; Bishop, D. M. *J. Chem. Phys.* **1998**, *108*, 1001.

(27) Luo, Y.; Ågren, H.; Jørgensen, P.; Mikkelsen, K. *Adv. Quantum Chem.* **1995**, *26*, 168.

(28) Levine, B. F.; Bethea, C. G. *J. Chem. Phys.* **1975**, *63*, 2666.

(29) Teng, C. C.; Garito, A. F. *Phys. Rev. B* **1983**, *28*, 6766.

(30) Stähelin, M.; Moylan, C. R.; Burland, D. M.; Willetts, A.; Rice, J. E.; Shelton, D. P.; Donley, E. A. *J. Chem. Phys.* **1993**, *98*, 5595.

(31) Willetts, A.; Rice, J. E. *J. Chem. Phys.* **1993**, *99*, 426.

(32) Yu, J.; Zerner, M. C. *J. Chem. Phys.* **1994**, *100*, 7487.

(33) Cammi, R.; Cossi, M.; Tomasi, J. *J. Chem. Phys.* **1996**, *104*, 4611.

(34) Cammi, R.; Cossi, M.; Mennucci, B.; Tomasi, J. *J. Chem. Phys.* **1996**, *105*, 10556.

(35) Mikkelsen, K. V.; Luo, Y.; Ågren, H.; Jørgensen, P. *J. Chem. Phys.* **1995**, *102*, 9362.

(36) Mikkelsen, K. V.; Jørgensen, P.; Jensen, H. J. A. *J. Chem. Phys.* **1994**, *100*, 6597.

(37) Mikkelsen, K. V.; Luo, Y.; Ågren, H.; Jørgensen, P. *J. Chem. Phys.* **1994**, *100*, 8240.

(38) Luo, Y.; Cesar, A.; Ågren, H. *Chem. Phys. Lett.* **1996**, *252*, 389.

(39) Mikkelsen, K. V.; Ruud, K.; Helgaker, T. *Chem. Phys. Lett.* **1996**, *253*, 443.

(40) Mikkelsen, K. V.; Luo, Y.; Ågren, H.; Jørgensen, P. *J. Chem. Phys.* **1995**, *102*, 9362.

(41) Keszthelyi, T.; Poulsen, T. D.; Ogilby, P. R.; Mikkelsen, K. V. *J. Phys. Chem. A* **2000**, *104*, 10550.

(42) Weldon, D.; Poulsen, T. D.; Mikkelsen, K. V.; Ogilby, P. R. *Photochem. Photobiol.* **1999**, *70*, 369.

(43) Keszthelyi, T.; Weldon, D.; Andersen, T. N.; Poulsen, T. D.; Mikkelsen, K. V.; Ogilby, P. R. *Photochem. Photobiol.* **1999**, *70*, 531.

(44) Medina-Llanos, C.; Ågren, H.; Mikkelsen, K. V.; Jensen, H. J. Aa. *J. Chem. Phys.* **1989**, *90*, 6422.

(45) Ågren, H.; Medina-Llanos, C.; Mikkelsen, K. V.; Jensen, H. J. Aa. *Chem. Phys. Lett.* **1989**, *153*, 322.

(46) Ågren, H.; Medina-Llanos, C.; Mikkelsen, K. V. *Chem. Phys.* **1987**, *115*, 43.

(47) Luo, Y.; Norman, P.; Ågren, H.; Sylvester-Hvid, K. O.; Mikkelsen, K. V. *Phys. Rev. E* **1998**, *57*, 57.

(48) Sylvester-Hvid, K. O.; Ratner, M. A.; Mikkelsen, K. V. *J. Phys. Chem.*, submitted for publication, 2004.

(49) Malkin, V. G.; Malkina, O. L.; Steinebrunner, G.; Huber, H. *Chem.−Eur. J.* **1996**, *2*, 452.

(50) Buckingham, A. D. In *Intermolecular Forces*; Hirschfelder, J. O., Ed.; *Advances in Chemical Physics 12*; Wiley: New York, 1967.

(51) Wallqvist, A.; Karlström, G. *Chem. Scr.* **1989**, *29A*, 131.

914 *J. Phys. Chem. A, Vol. 109, No. 5, 2005*

Sylvester-Hvid et al.

(52) Åstrand, P.-O.; Wallqvist, A.; Karlström, G. *J. Chem. Phys.* **1994**, *100*, 1262.

(53) Åstrand, P.-O.; Linse, P.; Karlström, G. *Chem. Phys.* **1995**, *191*, 195.

(54) Åstrand, P.-O.; Wallqvist, A.; Karlström, G. *J. Phys. Chem.* **1994**, *98*, 8224.

(55) Buckingham, A. D. *Can. J. Chem.* **1960**, *38*, 300.

(56) Batchelor, J. G. *J. Am. Chem. Soc.* **1975**, *97*, 3410.

(57) Nymand, T. M.; Åstrand, P.-O.; Mikkelsen, K. V. *J. Phys. Chem. B* **1997**, *101*, 4105.

(58) Nymand, T. M.; Åstrand, P.-O. *J. Chem. Phys.* **1997**, *106*, 8332.

(59) Nymand, T. M.; Åstrand, P.-O. *J. Phys. Chem. A* **1997**, *101*, 10039.

(60) Wagnière, G. H. *Linear and Nonlinear Optical Properties of Molecules*; Verlag Helvetica Chimica Acta: Basel, Switzerland, 1993.

(61) Fiutak, J. *Can. J. Phys.* **1963**, *41*, 12.

(62) Armstrong, J. A.; Bloembergen, N.; Ducuing, J.; Pershan, P. S. *Phys. Rev.* **1962**, *127*, 1918.

(63) Mikkelsen, K. V.; Sylvester-Hvid, K. O. *J. Phys. Chem.* **1996**, *100*, 9116.

(64) Olsen, J.; Jørgensen, P. *J. Chem. Phys.* **1985**, *82*, 3235.

(65) Reis, H.; Papadopoulos, M. G.; Theodorou, D. N. *J. Chem. Phys.* **2001**, *114*, 876.

(66) Reis, H.; Papadopoulos, M. G.; Calaminici, P.; Jug, K.; Koster, A. M. *Chem. Phys.* **2000**, *261*, 359.

(67) Janssen, R. H. C.; Theodorou, D. N.; Raptis, S.; Papadopoulos, M. G. *J. Chem. Phys.* **1999**, *111*, 9711.

(68) Partington, J. R. *An Advanced Treatise on Physical Chemistry*; Longmans: London, 1953; Vol. 4.

(69) Jensen, L.; Åstrand, P.-O.; Sylvester-Hvid, K. O.; Mikkelsen, K. V. *J. Phys. Chem. A* **2000**, *104*, 1563.

(70) Jensen, L.; Åstrand, P.-O.; Osted, A.; Kongsted, J.; Mikkelsen, K. V. *J. Chem. Phys.* **2002**, *116*, 4001.

(71) Jensen, L.; Åstrand, P.-O.; Mikkelsen, K. V. *J. Phys. Chem. B* **2004**, *108*, 8226.

(72) Press, W. H.; Teukolsky, S. A.; Vetterling, W. T.; Flannery, B. P. *Numerical Recipes*; Cambridge university Press: Cambridge, U.K., 1992.

(73) Mikkelsen, K. V.; Ågren, H.; Jensen, H. J. A.; Helgaker, T. *J. Chem. Phys.* **1988**, *89*, 3086.

(74) Mikkelsen, K. V.; Jørgensen, P.; Jensen, H. J. A. *J. Chem. Phys.* **1994**, *100*, 6597.

(75) Mikkelsen, K. V.; Dalgaard, E.; Swanstrøm, P. *J. Phys. Chem.* **1987**, *91*, 3081.

(76) Åstrand, P.-O.; Linse, P.; Karlström, G. *Chem. Phys.* **1995**, *191*, 195.

(77) Linse, P.; Wallqvist, A.; Åstrand, P.-O.; Nymand, T. M.; Lobaskin, V. *MOLSIM*, version 2.1.20; Lund University: Lund, Sweden, 1998.

(78) Ahlström, P.; Wallqvist, A.; Engström, S.; Jönsson, B. *Mol. Phys.* **1989**, *68*, 563.

(79) Berendsen, H. J. C.; Postma, J. P. M.; van Gunsteren, W. F.; DiNola, A.; Haak, J. R. *J. Chem. Phys.* **1984**, *81*, 3684.

(80) Allen, M. P.; Tildesley, D. S. *Computer Simulations of Liquids*; Clarendon: Oxford, U.K., 1987.

(81) Swope, W. C.; Andersen, H. C.; Berens, P. H.; Wilson, K. R. *J. Chem. Phys.* **1982**, *76*, 637.

(82) Helgaker, T.; Jensen, H. J. A.; Joergensen, P.; Olsen, J.; Ruud, K.; Aagren, H.; Auer, A.; Bak, K.; Bakken, V.; Christiansen, O.; Coriani, S.; Dahle, P.; Dalskov, E. K.; Enevoldsen, T.; Fernandez, B.; Haettig, C.; Hald, K.; Halkier, A.; Heiberg, H.; Hettema, H.; Jonsson, D.; Kirpekar, S.; Kobayashi, R.; Koch, H.; Mikkelsen, K. V.; Norman, P.; Packer, M. J.; Pedersen, T. B.; Ruden, T. A.; Sanchez, A.; Saue, T.; Sauer, S. P. A.; Schimmelpfennig, B.; Sylvester-Hvid, K. O.; Taylor, P. R.; Vahtras, O. *DALTON, a molecular electronic structure program*, release 1.2; 2001.

(83) Widmark, P.-O.; Malmqvist, P.-Å.; Roos, B. O. *Theor. Chim. Acta* **1990**, *77*, 291.

(84) Pierloot, K.; Dumez, B.; Widmark, P.-O.; Roos, B. O. *Theor. Chim. Acta* **1995**, *90*, 87.

(85) Thormahlen, I.; Straub, J.; Grigull, U. *J. Phys. Chem. Ref. Data* **1985**, *14*, 933.

(86) Osted, A.; Kongsted, J.; Mikkelsen, K. V.; Christiansen, O. *Mol. Phys.* **2003**, *101*, 2055.

(87) Kongsted, J.; Osted, A.; Mikkelsen, K. V.; Christiansen, O. *J. Phys. Chem. A* **2003**, *107*, 2578.

(88) Kongsted, J.; Osted, A.; Mikkelsen, K. V.; Christiansen, O. *J. Chem. Phys.* **2003**, *118*, 1620.

(89) Reis, H.; Raptis, S. G.; Papadopoulos, M. G. *Chem. Phys.* **2001**, *263*, 301.

(90) Luis, J. M.; Duran, M.; Andrés, J. L.; Champagne, B.; Kirtman, B. *J. Chem. Phys.* **1999**, *111*, 875.

(91) Luis, J. M.; Duran, M.; Andrés, J. L. *J. Chem. Phys.* **1997**, *107*, 11501.

(92) Macak, P.; Norman, P.; Luo, Y.; Ågren, H. *J. Chem. Phys.* **2000**, *112*, 1868.